A pathogenic HEXA missense variant in wild boars with Tay-Sachs disease.

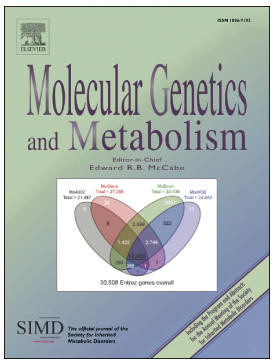

A pathogenic HEXA missense variant in wild boars with Tay-Sachs disease

Valeria Bertani, Simona Prioni, Rosanna Di Lecce, Ferdinando Gazza, Luisa Ragionieri, Giuseppe Merialdi, Paolo Bonilauri, Vidhya Jagannathan, Sara Grassi, Livia Cabitta, Antonella Paoli, Amelia Morrone, Sandro Sonnino, Cord Drögemüller, Anna Maria Cantoni

PII: S1096-7192(21)00702-2

DOI: https://doi.org/10.1016/j.ymgme.2021.05.001

Reference: YMGME 6768

To appear in: *Molecular Genetics and Metabolism*

Received date: 23 October 2020

Revised date: 2 May 2021

Accepted date: 3 May 2021

Please cite this article as: V. Bertani, S. Prioni, R. Di Lecce, et al., A pathogenic HEXA missense variant in wild boars with Tay-Sachs disease, *Molecular Genetics and Metabolism* (2018), https://doi.org/10.1016/j.ymgme.2021.05.001

A pathogenic *HEXA* missense variant in wild boars with Tay-Sachs disease

Valeria Bertani[a,1,2], Simona Prioni[b,2], Rosanna Di Lecce[a], Ferdinando Gazza[a], Luisa Ragionieri[a], Giuseppe Merialdi[c], Paolo Bonilauri[c], Vidhya Jagannathan[d], Sara Grassi[b], Livia Cabitta[b], Antonella Paoli[e], Amelia Morrone[e,f], Sandro Sonnino[b], Cord Drögemüller[d,2], Anna Maria Cantoni[a,2]

[a]Department of Veterinary Science, University of Parma. Via Taglio, 8, 43100 Parma PR (Italy)

[b]Department of Medical Biotechnology and Translational Medicine, University of Milano. Via Fratelli Cervi 93, 20129 Segrate (Mi) (Italy)

[c]Istituto Zooprofilattico Sperimentale della Lombardia e dell'Emilia Romagna. Via Pietro Fiorini, 5, 40127 Bologna BO (Italy)

[d]Institute of Genetics, Vetsuisse Faculty, University of Bern, Bremgartenstrasse 109a, 3001 Bern (Switzerland)

[e]Molecular and Cell Biology Laboratory, Paediatric Neurology Unit and Laboratories, Neuroscience Department, A. Meyer Children's Hospital, Florence, Italy

[f]Department of Neurosciences, Psychology, Pharmacology and Child Health, University of Florence, Italy

[*]Corresponding author.

Abstract

[1] Present address: Bayer SAS, 355 rue Dostoïevski, 06906 Sophia Antipolis (France)
[2] These authors contributed equally to this work

Gangliosidoses are inherited lysosomal storage disorders caused by reduced or absent activity of either a lysosomal enzyme involved in ganglioside catabolism, or an activator protein required for the proper activity of a ganglioside hydrolase, which results in the intra-lysosomal accumulation of undegraded metabolites. We hereby describe morphological, ultrastructural, biochemical and genetic features of GM2 gangliosidosis in three captive bred wild boar littermates. The piglets were kept in a partially-free range farm and presented progressive neurological signs, starting at 6 months of age. Animals were euthanized at approximately one year of age due to their poor conditions. Neuropathogens were excluded as a possible cause of the signs. Gross examination showed a reduction of cerebral and cerebellar consistency. Central (CNS) and peripheral (PNS) nervous system neurons were enlarged and foamy, with severe and diffuse cytoplasmic vacuolization. Transmission electron microscopy (TEM) of CNS neurons demonstrated numerous lysosomes, filled by parallel or concentric layers of membranous electron-dense material, defined as membranous cytoplasmic bodies (MCB). Biochemical composition of gangliosides analysis from CNS revealed accumulation of GM2 ganglioside; furthermore, Hex A enzyme activity was less than 1% compared to control animals. These data confirmed the diagnosis of GM2 gangliosidosis. Genetic analysis identified, at a homozygous level, the presence of a missense nucleotide variant c.1495C > T (p.Arg499Cys) in the hexosaminidase subunit alpha gene (*HEXA*), located within the GH20 hexosaminidase superfamily domain of the encoded protein. This specific *HEXA* variant is known to be pathogenic and associated with Tay-Sachs disease in humans, but has never been identified in other animal species. This is the first report of a *HEXA* gene associated Tay-Sachs disease in wild boars and thus provides a comprehensive description of a novel spontaneous animal model for this lysosomal storage disease.

Keywords

Tay-Sachs disease, lysosomal storage disease, *HEXA,* GM2, wild boar, swine, whole-genome sequencing.

1. Introduction

The GM2-gangliosidoses are genetic diseases caused by impaired degradation of ganglioside GM2 and related glycolipids, such as GalNAc-GD1a[1], particularly within neuronal cells. GM2 is a minor component of the brain ganglioside mixture, but it is formed in lysosomes by removal of galactose from GM1 ganglioside. It is then degraded by cleavage of the β-glycosidic linkage between the N-acetylgalactosaminyl residue and the galactose residue by β-hexosaminidase, which requires the presence of the GM2 activator protein[2].

There are three isoenzymes of β-hexosaminidase. The first Hex A, consisting of two subunits (α and β), cleaves off terminal β-glycosidically linked N-acetylglucosamine and N-acetylgalactosamine residues from negatively charged and uncharged glycoconjugates; this enzyme has two active sites on the α and β-chain. The second isoenzyme, Hex B, a homodimer of β subunits, predominantly cleaves uncharged substrates, like glycolipid GA2 and oligosaccharides with terminal N-acetylhexosamine residues; it has two active sites at the homodimer interface. A third isoenzyme, Hex S (αα) is of secondary significance for GM2 degradation, but it contributes to the degradation of glycosaminoglycans and sulfated glycolipids[2].

Defects in genes coding for α-chain (*HEXA*) or β-chain (*HEXB*) of the β-hexosaminidase isoenzymes, as well as GM2-activator (*GM2A*), can lead to impairment of GM2 ganglioside catabolism and its pathological accumulation.

Moreover, there are four biochemical variants of GM2 gangliosidosis: Tay-Sachs disease (variant B), resulting from variants of the *HEXA* gene and associated with deficient activity of isoenzyme Hex A but normal Hex B; variant B1, resulting from variants of the *HEXA* gene and associated with deficient activity of isoenzyme Hex A, in this case catalytically inactive against the GM2 ganglioside but active with neutral substrate; Sandhoff disease (variant O), resulting from variants of the *HEXB* gene and associated with deficient activity of both isoenzyme Hex A and Hex B; GM2 activator deficiency (variant AB) due to variant of the *GM2A* gene and characterized by normal isoenzyme Hex A and Hex B but inability to form a functional GM2-GM2 activator complex[3,4]. Currently, 149 pathogenic and likely-pathogenic genetic human variants affecting the *HEXA* gene have been described[5].

Spontaneous animal models of gangliosidosis have been studied in order to identify similarities with human disease, to understand the its pathogenesis and to develop potential therapies[6]. Murine models of Tay–Sachs disease have been generated using gene targeting techniques; although, in rodents, sialidases are able to convert GM2 to GA2. Thus, this alternative catabolic pathway for GM2 ganglioside is responsible for a Tay–Sachs knock-out model that does not recapitulate the human conditions faithfully[7,8] . In veterinary medicine, spontaneous GM2 gangliosidosis has been described as autosomal recessive disorder in different animal species such as feline (https://omia.org/OMIA000403/9685/), canine (Japanese chin, https://omia.org/OMIA001461/9615/)[9], ovine (Jacob breed, https://omia.org/OMIA001461/9940/)[10,11], lagomorph (rabbit, https://omia.org/OMIA001461/9986/)[12], porcine (Yorkshire breed, https://omia.org/OMIA000403/9823/)[13], avian (American flamingo, https://omia.org/OMIA001461/9217/)[14] and wild ruminant (Muntjak deer, https://omia.org/OMIA001461/9888/)[15].

So far, the underlying causative genetic defect has only been detected in Japanese chin dogs (*HEXA* missense variant [16]), Jacob sheep (*HEXA* splice site variant[10]) and flamingos (*HEXA* missense variant[14]). Large animal models for gangliosidosis, in which the size and complexity of the brain are more similar to humans, have allowed a comparison of different CNS delivery methods for safety, distribution and efficacy of potential therapeutics. Moreover, in respect to mouse models, these species also have more heterogeneity in genetic backgrounds, which more accurately mimics human populations[6,17].

Particularly, Jacob sheep model examinations have given important insights into these genetic diseases[17] and the model has been tested with adeno-associated virus gene therapy, giving promising results[18,19].

In the present study, spontaneous Tay-Sachs disease in wild boars was demonstrated investigating three wild boars littermates, that developed progressive neurological signs. Pathological, ultrastructural, biochemical, and genetic findings, consistent with naturally occurring Tay–Sachs disease, have been demonstrated in these wild boars, suggesting a potential role as spontaneous models.

2. Materials and Methods

2.1. Wild boar cases and pedigree information

We examined four littermate piglets, one asymptomatic and three symptomatic, from the same litter hailing form the same partial free-range farm. For case 1 necropsy, histology, immunohistochemistry, transmission electron microscopy, biochemical analysis as well as whole-genome sequencing have been performed. For case 2, as the previous, genetic analysis, with *HEXA* genotyping. For case 3, who has been referred, only bacteriological and virologic analysis, histology and immunohistochemistry

have been performed. A normal asymptomatic littermate boar was used as control (Fig 6A).

2.2. Clinical signs, necropsy and microbiological investigations

Piglets presented progressive neurological signs, starting at 6 months of age. Animals were clinically monitored by a veterinarian and, due to their progressive poor conditions, euthanasia was decided. Wild boars were injected intramuscularly with sedative and euthanized by intravenous barbiturate overdose (technique consistent with the AVMA Guidelines on Euthanasia [20]) at approximately one year of age. For case 1 and 2, during necropsies, gross examination was performed and tissue specimens were collected for histology; further brain samples were harvested for TEM and biochemical investigation. Blood samples were collected for genetical analysis. For case 3, tissue samples from brain, spleen and liver were submitted for bacteriological culture, on blood agar and MacConkey agar media and incubated for 72 h at 37° C. Tissue samples from brain (trigeminal ganglion, olfactory bulb, brain stem) were PCR tested for Porcine herpesvirus-1 and Classic Swine Fever virus[21,22].

2.3. Histology, histochemistry and immunohistochemistry

Tissue specimens were fixed in phosphate buffered formalin, pH 7.4 (10% v/v) immediately after organs removal, processed routinely, embedded in paraffin, sliced at 3 µm and stained with hematoxylin and eosin (HE), periodic acid Schiff (PAS) and luxol fast blue (LFB). Immunohistochemistry (IHC) was performed with standard avidin-biotin-peroxidase complex (ABC) procedure with a commercial kit (Vectastain Standard Elite; Vector Laboratories, Burlingame, California, USA). Primary monoclonal antibodies used included anti-GFAP (1:400 dilution; Sigma-Aldrich), and anti-vimentin (1:50 dilution; Dako). Labelling was visualized with 3,3'-Diaminobenzidine (DAB) and counterstained with

Mayer's hematoxylin. Negative controls were performed replacing the primary antibodies with phosphate buffered saline[23]. Slides were examined using a Nikon Eclipse E800 microscope (Nikon Corporation, Japan) with Nikon PLAN APO lenses and equipped with Camera DIGITAL SIGHT DS-Fi1 (Nikon Corporation, Japan) acquiring pictures with DS camera control unit DS-L2 (Nikon Corporation, Japan).

2.4. Resin sections and transmission electron microscopy (TEM)

Tissues were fixed in 2.5% glutaraldehyde / 0.1M PBS buffer pH 7.2 for 1 hour and dehydrated through the graded series of acetone and embedded in Durcupan (Fluka Chemie, Buchs, Switzerland). The polymerization occurred after 24 hours at 65°C. Sections of 2 µm were prepared using ultramicrotome Reichert (PabischWien), stained with Toluidine blue 0.5% sodium carbonate, and observed under light microscope. Ultrathin sections (~ 70 nm) were cut with a diamond blade, gathered on slotted copper grills, stained with 3% uranyl acetate and lead citrate and observed by a JEOL (JEM 2200 FS) transmission electron microscope operated at 80 KeV (Tokyo, Japan)[24]. Quantitative morphometry, based on transmission electron microscopy images, was performed to the detect the diameter and interlamellar periodicity of intracytoplasmic accumulations[25], using ImageJ software[26,27].

2.5. Biochemical analyses

2.5.1 Biochemical lipids assays

Brain tissue samples (2-3 g) were collected from cortex, thalamus, medulla oblongata, and cerebellum during necropsy, and stored at -185 °C. Samples were thawed on ice (4°C). Meninges were removed, tissues were minced with a surgical blade, re-suspended in ice-cold water, sonicated, then Dounce homogenized (10 strokes, tight), snap frozen and lyophilized. Lipids from the

lyophilized samples were added with 1550 µL $CHCl_3/CH_3OH/H_2O$ 20:10:1 (v/v/v), mixed at 1100 rpm, (room temperature, RT) for 15 minutes and centrifuged at 16,100xg, at RT for 15 minutes. The supernatant was collected as total lipid extract (TLE) and extraction was repeated twice again by adding 1550 µL of the solvent system to pellets. Pellets were air dried, suspended in 1M NaOH, incubated overnight at RT before dilution with water to 0.05M NaOH, to allow the determination of the protein content with DC assay. Aliquots of the TLE were subjected to a modified two-phase Folch's partitioning by adding 20% of water by volume, yielding the aqueous (Aq.Ph.) and the organic phases (Or.Ph.). The samples were mixed at 1100 rpm, RT for 15 minutes and centrifuged at 16,100xg, for 15 minutes at RT. The Aq.Ph. were recovered, CH_3OH/H_2O 1:1 (v/v) was added to the organic phase and samples were mixed at 1100 rpm, RT for 15 minutes and centrifuged at 16,100xg, for 15 minutes at RT. The new Aq.Ph. were recovered and pooled to previous ones. The Aq.Ph. were dried under N_2 flux, residues were suspended in water, dialyzed and then lyophilized. The Or.Ph. were dried under N_2 flux and residues were suspended in a known volume of $CHCl_3/CH_3OH$ 2:1. Aliquots of the Or.Ph. were then subjected to alkali treatment to remove glycerophospholipids. They were dried under N_2 flux, the residue was suspended in 100 µl 0.6 M NaOH in CH_3OH and incubated at 37°C overnight. The reaction was blocked by adding 120 µl 0.5 M HCl in CH_3OH. Reaction mixtures were phase separated by adding 1,050 µl of $CHCl_3/CH_3OH/H_2O$ 70:18:17), and the alkali-treated organic phases were used for TLC analysis. To determine endogenous lipid content, the various samples were analyzed by mono-dimensional silica gel high performance thin layer chromatography (HPTLC) using different solvent systems. The total lipid extracts were analyzed using $CHCl_3/CH_3OH$/0.2% aqueous $CaCl_2$ 60:35:8 (v/v/v) as a solvent system; the Aq.Ph. were analyzed with $CHCl_3/CH_3OH$/0.2% aqueous $CaCl_2$ 50:42:11 (v/v/v); the Or.Ph. and the alkali-treated Or.Ph. were

analyzed using $CHCl_3/CH_3OH/H_2O$ 110:40:6 (v/v/v). After separation, lipids were detected by spraying TLC plates with different colorimetric reagents (anisaldehyde, Ehrlich's reagent). Identification of lipids after separation and chemical detection was assessed by co-migration with lipid standards [28].

2.5.2. Biochemical enzyme assays

Hex A enzyme activity was assayed in lymphocytes of affected and control animals using the fluorogenic substrate, 4-Methylumbelliferyl-6-sulfo-N-acetyl-β-D-glucosaminide, Potassium Salt – Calbiochem, The assay was carried out with Krasse et al method [29] adapted by Moscerdam Substrates/ Carbosynth. β-galactosidase and total Hex (A+B) enzyme activities, as internal controls, were assayed in all tested samples as previously reported[30,31]. The Bicinchoninic acid (BCA) method was used to determine samples' protein concentration. Lysosomal enzymatic activity was expressed as nanomoles of substrate hydrolyzed per milligram of total protein per hour. All assays were performed in triplicate.

2.6. Whole-genome sequencing and polymerase chain reaction (PCR)

Genomic DNA was isolated from EDTA stabilized blood samples using the Maxwell RSC instrument (Promega, Madison, WI, USA). Whole-genome sequencing information at 16x coverage was obtained from one affected animal (case 1) using a HiSeq3000 instrument (Illumina, San Diego, CA, USA) and 2 x 150bp paired-end reads. The sequence data analysis was performed as previously described [32]. The genome sequencing data of the sequenced animal were deposited in the European Nucleotide Archive (ENA, https://www.ebi.ac.uk/ena) under accession number SAMEA5059492. The sequence data of the affected wild boar of case 1 were compared to a reference genome (GenBank Sscrofa11.1) and 4 available control animals (2

purebred Duroc and 2 crossbred Piétrain x Swiss Landrace); deposited in the ENA under study accession numbers SAMEA5059488-SAMEA5059491.

Primers for the amplification of the point mutation [forward GTGCCTAAGCAAGAGGCTGT (chr 7 g.60910209-60910228); reverse GTCAGTAAGGGCTCCTCAGC (chr 7 g.60910422-60910441)] were designed using the Primer3 software (https://primer3.sourceforge.net). The given genome location of these primers for amplification of a 233 bp PCR product are based on the Sscrofa11.1 pig genome assembly. After PCR amplification, direct Sanger sequencing of the obtained products was performed on the 3730 DNA-Analyzer (Thermofisher, Darmstadt, Germany). The resulting chromatogram and the relative nucleotide sequence were analyzed with Sequencher 5.1 software (GeneCodes, Ann Arbor, USA).

3. Results

3.1. Clinical signs, necropsy and microbiological investigations

Case 1 and 2 were in poor body conditions and had progressive neurological signs, consisting with behavioral changes, dysmetria and ataxia, and culminating with involuntary twitching, seizures, quadriplegia and lateral decubitus. On necropsy examination, gross lesions were scant in both cases: brain was characterized by swelling, reduction in consistency of cerebral and cerebellar parenchyma and moderate meningeal congestion; severe diffuse hepatic degeneration, gastric and intestinal dilation were also evident. For case 3, bacteriology and PCR analysis for Porcine herpesvirus-1 and Classical swine fever virus were negative.

3.2. Histopathology, histochemistry and immunohistochemistry

In all 3 affected animals, brain, cerebellum and peripheral ganglia showed diffusely perikaryal enlargement. Neurons, up to 50 microns, had a rounded and distinct cell outline. The cytoplasm of neurons was abundant and

appeared faintly eosinophilic to foamy vacuolated; cytoplasmic vacuolizations were variably in size, ranging from a minimum of 2-3 micron up to the maximum of 10-15 micron, filled with pale eosinophilic granular material or optically clear. Multifocally, neurons showed shrunken and hyperchromatic nuclei with pyknotic dense chromatin. Moreover, nuclei moved from the center to the plasma membrane, defined as central chromatolysis (Fig.1A). Diffusely, numerous round swollen axons (spheroids and ellipsoids), characterized by variable loosely granular to densely eosinophilic appearance, were evident. Multifocally, the axon hillock was enlarged to accommodate the stored material, forming meganeurites; moreover, Purkinje cell dendrites were multifocally thickened. Numerous glial cells were diffusely evident throughout the cerebral parenchyma and were recognizable as astrocytes or gemistocytes. Gitter cells were arranged in aggregates (glial nodules) close to neurons as perineuronal satellite lymphocytes (satellitosis). Virchow–Robin spaces were expanded by the presence of edema. The same neuronal cytoplasmic storage, associated to moderate gliosis and astrocytosis, was identified in ventral and dorsal horn neurons of the spinal cord as well as in peripheral ganglia. Retinal ganglion cells were also affected by vacuolation of inner and outer plexiform layers with disarray and reduction of inner and outer nuclear layers (Fig.1B).

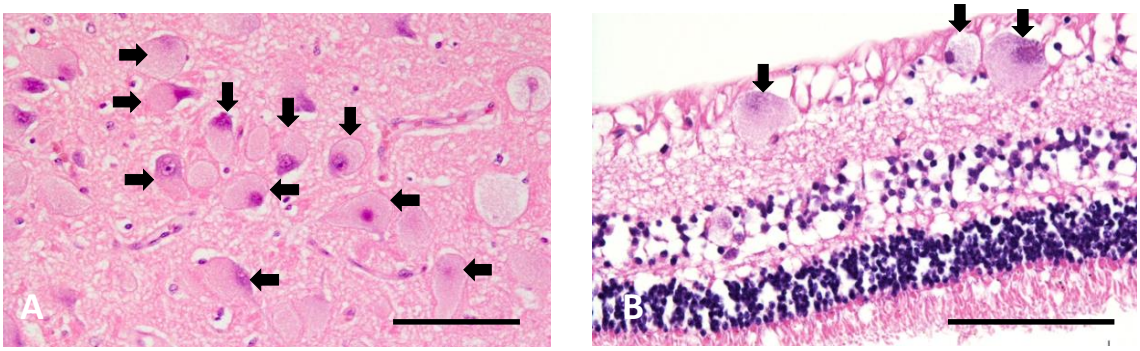

Figure 1. Histological sections of Cerebrum and Retina
(A) Brain, Cortex – Case 1. Neurons, indicated by arrows, appeared severely enlarged with finely faintly eosinophilic granular to foamy vacuolated cytoplasm. Many neurons showed a peripheral displacement of the nucleus

and central chromatolysis. H&E, scale bar 100µm. (B) Eye, Retina – Case 1. Retinal ganglion cells, indicated by arrows, showed severe foamy vacuolation of cytoplasm of inner and outer plexiform layer with disarray and reduction of inner and outer nuclear layer. H&E, scale bar 100 µm.

Cytoplasmic neuronal vacuolation showed variable positivity for PAS staining; LFB staining revealed severe diffuse demyelination of the white matter in brain and spinal cord of affected animals compared to normal CNS (Fig.2A-B). Moreover, hepatocytes and Kupffer cells were characterized by finely diffusely vacuolated cytoplasm.

IHC for GFAP (Fig. 2C-D) identified astrocyte characterized by proliferation, hypertrophy and pronounced overlap of their processes. IHC for Vimentin (Fig. 2E-F) demonstrated the presence of numerous positive astrocytes; these were frequently intermingled and adjacent to cortical neurons, uniformly distributed or forming small aggregates especially in the white matter.

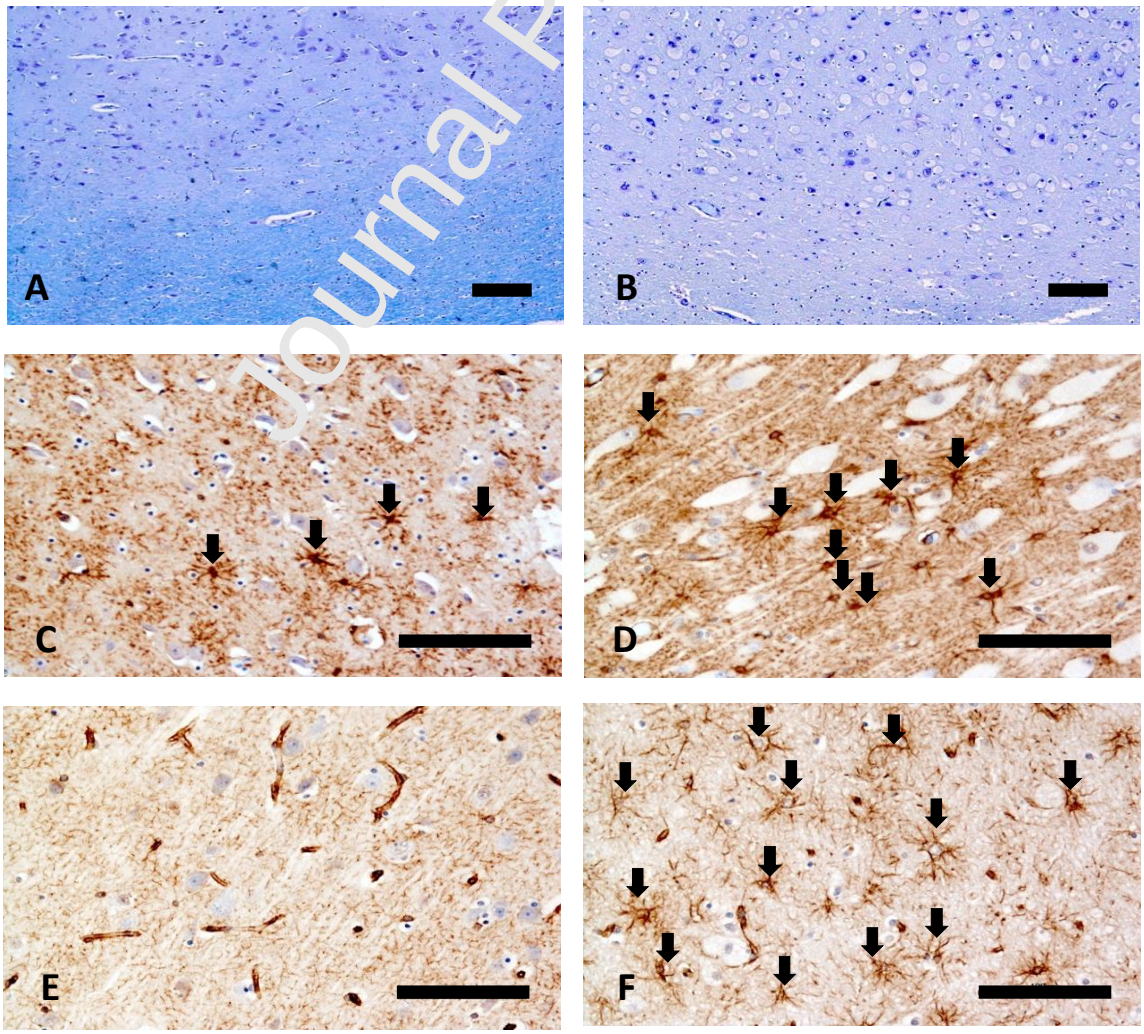

Figure 2. Histochemical stainings for myelin and IHC for GFAP and Vimentin

(A,C,E) Brain, somatosensory cortex – Control. Normal aspect. (B) Brain, somatosensory cortex – Case 2. White matter showed severe reduction of myelination (Luxol fast blue, scale bar 200 μm). (D) Brain, somatosensory cortex – Case 2. IHC for GFAP showed proliferating astrocytes, indicated by arrows, with cell body hypertrophy and overlap of astrocytic processes (IHC-DAB, scale bar 100 μm). (F) Brain, somatosensory cortex – Case 2. Many astrocytes, indicated by arrows, showed immunopositivity for vimentin intermediate filament (IHC-DAB, scale bar 100 μm).

3.3. Ultrastructural Findings

Transmission electron microscopy of cerebral cortex tissue confirmed, at low magnification, the presence of numerous swollen and degenerated neurons; these were characterized by discontinuous cellular membrane and multifocal loss of distinction of cellular margins. Cytoplasm was severely enlarged by numerous lysosomes, filled by membranous electrondense material, defined as membranous cytoplasmic bodies (MCB) (Fig.5A). These contained membranous material in single or multiple layers of concentric outer membranes surrounding inner components of short, straight or curved membranes. MCB size ranged from 0.6 up to 1.0 μm and average interlamellar periodicity was 33 ± 1 nm. Cytoplasm was also characterized by the presence of numerous large, round, double membrane bound, swollen mitochondria with reduced electrondensity of the matrix and loss of mitochondrial cristae (mitochondrial swelling and cristolysis). Nucleus was characterized by discontinuous nuclear membrane, and contained multiple scattered aggregates of electrondense heterochromatin along the nuclear envelope (chromatin margination) and dispersed granular electron-lucent euchromatin (Fig.5B).

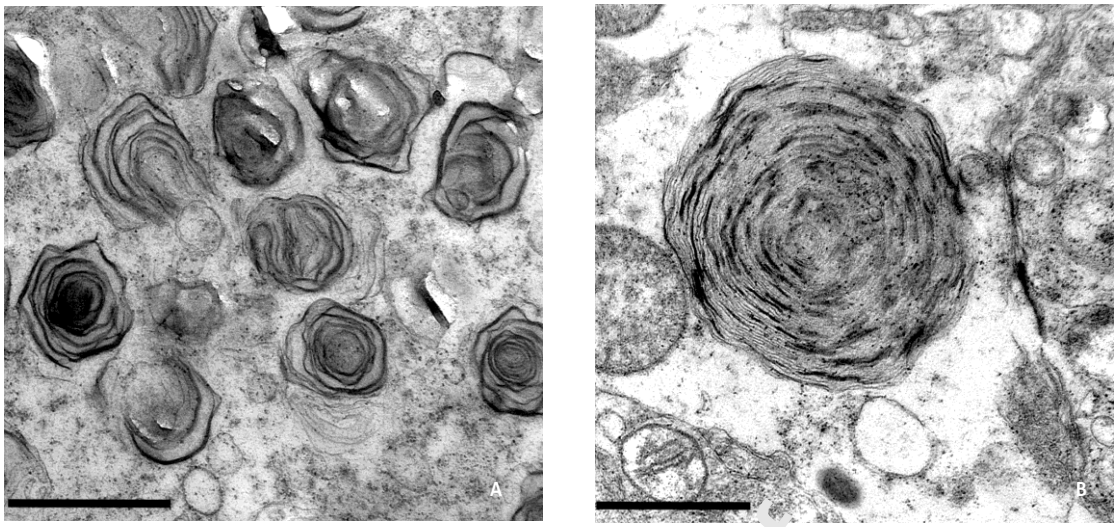

Figure 3. Transmission electron micrographs of case 1
(A) Brain, Cortex – Case 1. Within the cytoplasm of a neuron there was numerous membranous cytoplasmic bodies (MCB) (TEM, scale bar 1 μm); (B) Brain, Cortex – Case 1. Higher magnification of a membranous body consisting by several parallel or concentric layers of membranous electrondense material, with variable interlamellar periodicity (TEM, scale bar 1 μm).

3.4. Biochemical analyses

3.4.1. Biochemical lipid assays

Total lipid portion was separated to obtain Aq.Ph and Or.Ph. Aq.Ph contains gangliosides, in virtue of their negative charge, and traces of neutral sphingolipids. Or. Ph originally contained neutral glycosphingolipids and phospholipids; it was then treated with alkali, in order to hydrolyze the phopholipids and subjected to partitioning to eliminate the water-soluble part. The resulting methanolyzed Or. Ph contained only few sphingolipids and sphingomyelin. Aq.Ph and Or.Ph were analyzed with high performance thin layer chromatography (HPTLC).

In Aq.Ph. of normal tissues, ganglioside GM2 was hardly detected. On the contrary, in affected animals it was a major component of the Aq. Ph, in all cerebral and cerebellar tissues. Furthermore, an increase of the GalNAc-GD1a was also observed (Fig .4).

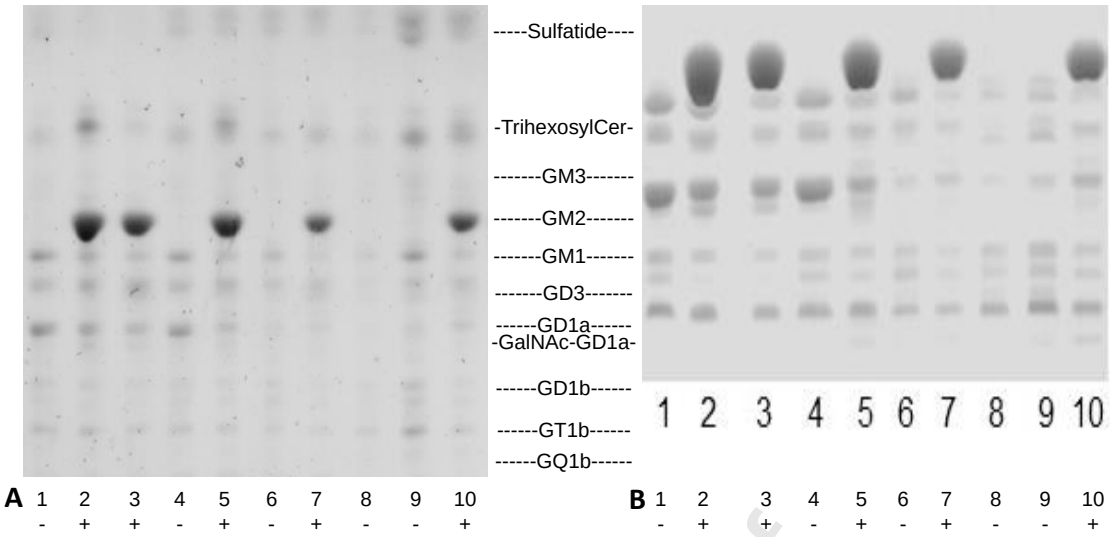

Figure 4: HPTLC mono-dimensional silica gel of Ac. Ph. of total brain lipid content

Increase of ganglioside GM2 and GalNAc-GD1a were observed in all examined cerebral and cerebellar locations of an affected animal (2, 3, 5, 7, 10).
(A) Solvent system chloroform/methanol/0.2% aqueous $CaCl_2$ 50:42:11 (v/v/v). Spray: Anisaldehyde (B) Solvent system chloroform/methanol/0.2% aqueous $CaCl_2$ 50:42:11 (v/v/v). Spray: Erlich.
For both A and B. Cortex: 1 control, 2-3 affected; Thalamus: 4 control, 5 affected; Medulla oblongata: 6 control, 7 affected; Cerebellum: 8-9 control, 10 affected.

In Or.Ph. of affected tissues, there was a drastic reduction of all principal components of myelin; particularly sphingomyelin, sulfatide and cerebrosides, which are present as doublets due to the heterogeneity of the lipid chains (hydroxylated and non-hydroxylated), were severely reduced. This was more severe for cortex and thalamus, compared to other anatomical locations.

Furthermore, an increase in trihexosylceramide was also evident (Fig.5)

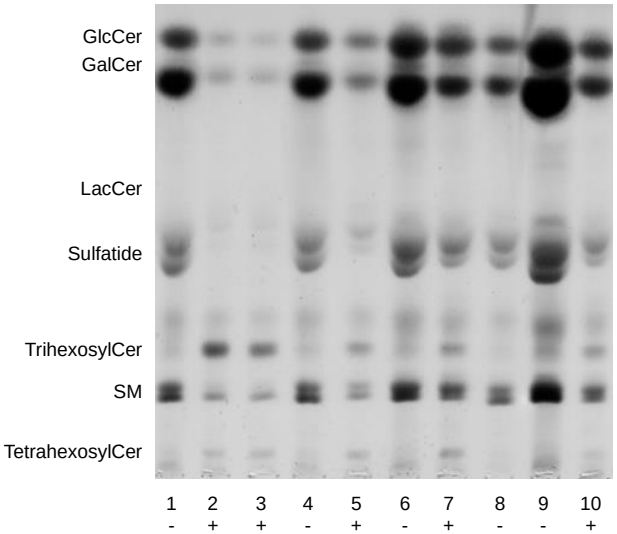

Figure 5: HPTLC mono-dimensional silica gel of methanolized Or. Ph. total brain lipid content

With variable severity in examined cerebral and cerebellar locations, Sphingomyelin (SM), Sulfatide and Cerebrosides (-Cer), were reduced, while an increase in Trihexosylceramide (TrihexosylCer) was also evident.
Solvent system chloroform/methanol/water 110:40:6 (v/v/v). Spray: Anisaldehyde.
Cortex: 1 control, 2-3 affected; Thalamus: 4 control, 5 affected; Medulla oblongata: 6 control, 7 affected; Cerebellum: 8-9 control, 10 affected.

3.4.2. Biochemical enzyme assays

Lysosomal Hex A enzyme activity in the lymphocytes of affected wild boars was almost absent [ranging from 0.01 to 0,7 nmol/mg prot/h] compared to the activity detected in control animals [ranging from 67-101 nmol/mg prot/h]. β-galactosidase and total Hex (A+B), performed as internal controls, were present with comparable values in all tested samples. Furthermore, the lysosomal enzyme activities tested in control animals, showed values comparable to human references.

3.5. Genetic analysis

The two most likely unaffected parents produced one litter of four piglets with three affected offspring [one male (case 1) and two females (cases 2 and 3)], and a presumed unaffected male. No pedigree information of the parents was available, neither their clear identification could be ruled out within the animals. Still, the limited pedigree data available suggests a monogenic autosomal recessive mode of inheritance (Fig. 6A), as the owner stated the possibility of a consanguineous mating. Whole genome sequencing of case 1 and subsequent variant analysis yielded a single variant (chr7:g.60910365C > T) that was predicted to affect the coding sequence of a functional candidate gene for Tay-Sachs disease (Fig 6B). Sanger sequencing confirmed the presence of this variant in case 1 and in case 2 (Fig. 6C) and its absence in the most likely unaffected littermate showing the wild type genotype. This private non-

synonymous variant in the *hexosaminidase subunit alpha* (*HEXA*) gene (NM_001123221.1:c.1495C > T) is located within the GH20 hexosaminidase superfamily domain of the encoded protein (Fig. 6D). It is predicted to alter the sequence of codon 499 resulting in the replacement of arginine by cysteine (p.Arg499Cys). The impact of a missense mutation depends on criteria such as the evolutionary conservation of an amino acid, the location and context within the protein sequence, and the biochemical consequence of the amino acid substitution[33]. The measurement of one or a combination of these criteria is used in various in silico algorithms that assess the predicted impact of a missense change; thus, software-based analysis of the HEXA p.Arg499Cys exchange characterized the variant as probably damaging (PolyPhen 2), deleterious (SIFT), pathogenic (MutPred2) or disease causing (Mutation Taster). Multiple species amino acid sequence alignment showed that the wild type residue at the affected position is conserved across *HEXA* orthologues in vertebrates including the zebrafish (Fig. 6D).

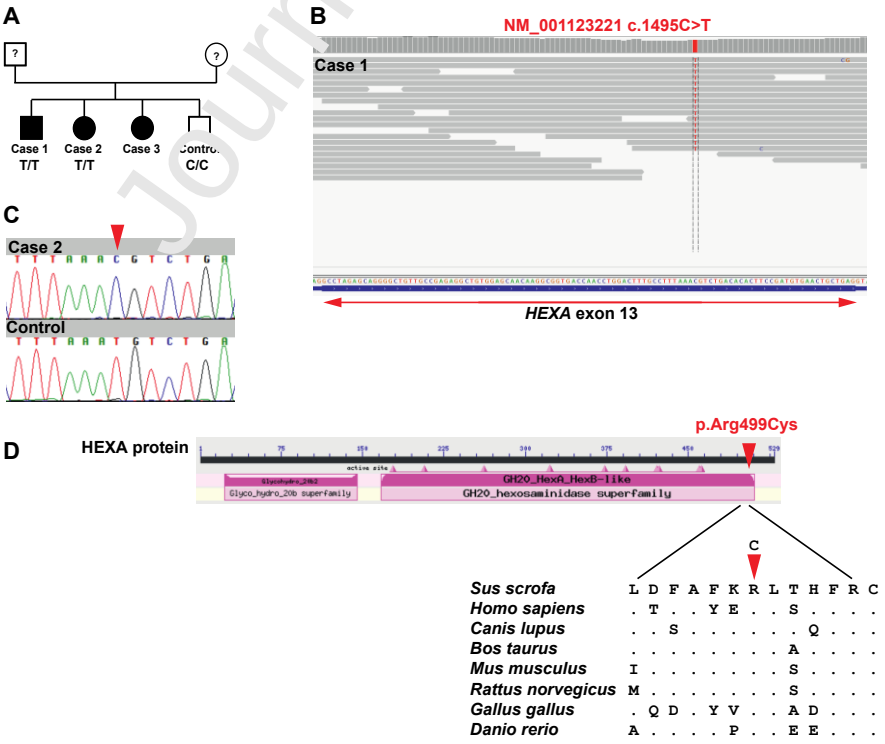

Figure 6: Genetic analysis of Tay-Sachs in wild boars

(A) Familial relationship of the three affected wild boars. Males are represented by squares, females by circles. Full shading designates affected animals. Animals with unknown phenotype are shown with question marks. (B) Integrative Genomics Viewer screenshot: Whole genome sequencing of an affected wild boar (case 1) revealed the presence of a homozygous single nucleotide variant in exon 13 of the *HEXA* gene on pig chromosome 7 (shown in red). (C) Chromatograms of case 2 and an unaffected littermate as control indicate the c.1495C > T variant which changes codon 499. (D). The variant is located in exon 13 of *HEXA* that encodes a functionally important domain of the HEXA protein. The predicted p.Arg499Cys exchange affects an evolutionary conserved residue. The multiple sequence amino acid alignment was done using accessions NP_001116693.1 (*Sus scrofa*), NP_000511.2 (*Homo sapiens*), XP_544758.2 (*Canis lupus familiaris*), NP_001068632.1 (*Bos taurus*), NP_034551.2 (*Mus musculus*), NP_001004435.1 (*Rattus norwegicus*), NP_001025561.1 (*Gallus gallus*), and NP_001017763.1 (*Danio rerio*).

4. Discussion

Gangliosides play a number of important roles in brain development and function, including receptor-mediated cell signaling, ion channel modulation, and dendritogenesis. They are found in the neuronal plasmalemma, where they co-localize with other glycosphingolipids and cholesterol in specialized areas of the membrane known as lipid domains or rafts[34]. Gangliosides can accumulate within lysosomes due to the defects in genes coding for two possible enzymes, β-Galactosidase and β-Hexosaminidase, causing GM1 and GM2 gangliosidosis respectively.

Clinically, human GM2 gangliosidosis can be sub-classified based on time of onset of neurological signs; particularly in the infantile form, children are normal at birth and show first symptoms, such as mild weakness, between 3 and 6 months of life. Hypotonia and acoustic hypersensitivity are among the most common early symptoms, followed by progressive hypertonia/spasticity, loss of hearing and diminished eyesight; seizures are late but common symptom[35]. A finding in most cases is a cherry red spot in the central retina of the patients, particularly in Tay-Sachs disease[3]. In the first months of the human disease, gross pathologic findings include brain atrophy, widening of the sulci, and mildly dilated ventricles[36]. The clinical findings of GM2 gangliosidosis in affected wild

boars are very similar to those described in human GM2 gangliosidosis; they were normal at birth with onset of neurological symptoms is the early life, during their development.

The histological findings in brain of affected wild boars were very similar to those described in human GM2 gangliosidosis, with neurons diffusely enlarged with round to ovoid shape, distended by foamy to granular cytoplasm, evident throughout the CNS and PNS. Spheroids are caused by accumulation of mitochondria, membrane-bound vesicles and dense bodies; particularly in lysosomal storage diseases, this is caused by axoplasmic transport defect or deprivation of key transport molecules. Furthermore, a striking correlation between the location and the incidence of axonal spheroids and the type and severity of clinical neurological disease, more than other morphological changes and cell death, has been demonstrated[37,38]. Meganeurites, defined as parasomatic enlargements within the axonal hillock, are multifocally evident secondary to storage; they contain storage cytosome[38] and are diffusely characterized by abnormally high densities of neurites. In human patients, an increased expression of GAP43, a phosphoprotein that promotes neurite formation during axonal growth and regeneration, correlates with an enhanced neuritogenesis. Increased neuritogenesis has been suggested to cause neuronal dysfunction in the GM2 gangliosidoses[39].

These pathological changes affecting neurons can lead to neuronal death; multifocally, angulated and hypereosinophilic neurons with shrunken nucleus, were evident throughout the brain. In human patients and mouse models, this appears to be mainly the result of apoptotic process, probably triggered by an alteration of calcium levels in the endoplasmic reticulum, resulting in an unfolded protein response[40]. Furthermore, elevated expression of cathepsin B, a lysosomal protease, has been shown to be released by activated microglia and to directly cause neuronal apoptosis[39].

Decreased and inhomogeneous myelin content was evident in the cerebral and cerebellar white matter of affected wild boars, compared with control tissue. The myelin basic protein gene, expressed by oligodendrocytes, was also significantly depressed in gene expression studies in patients affected by GM2 gangliosidosis[39]. The causes of myelin decrease are still under investigation, but several studies have confirmed direct metabolic effects on oligodendrocytes contributing to delayed or abnormal myelination (dysmyelinogenesis). Both primary effect of the metabolic disease on normal oligodendroglial growth and function, as well as a secondary influence of aberrant neuroaxonal development on myelination have been proposed as possible mechanisms[41]. Reactive astrocytosis was also associated with neuronal loss. Normally, astrocytes have non overlapping processes and are characterized by presence of vimentin intermediate filament in their immature stages, while mature astrocytes express GFAP only[42–44]. In affected wild boars, astrocytes were characterized by increased GFAP content; moreover, they were hypertrophic with areas of overlap of their processes and scattered areas of aggregation, especially in cortical areas. Furthermore, hypertrophied astrocytes were characterized by increase vimentin content, particularly, these astrocytes were frequently associated to vacuolated cortical neurons. All these findings can be defined as mild to moderate reactive astrogliosis[44]. The same findings were also evident in gene expression profiles of astrocytes from affected human patients [39]. Severe astrocytic expression of vimentin has been interpreted as a transient reversion to an immature phenotype or as a recruitment of immature astrocytes[44–46].

During disease development, activation of microglia in affected animals is milder compared to human, although the role it plays in the pathogenesis is still unclear. In human patients, a large fraction of the most elevated genes expressed could be attributed to activated macrophages/microglia and

astrocytes. All these findings confirm that gangliosidosis, as a model of neurodegeneration, includes inflammation as a factor leading to the precipitous loss of neurons[39].

TEM demonstrate intracytoplasmic presence of a large number of MCB, referable to the ultrastructural aspects of the lysosomal inclusions characteristic for gangliosidosis[24,47]. These are membrane-bound lysosomes distended with membranous material arranged in concentric circles or lamellae. The core of the bodies may contain finely granular amorphous material, as well as coarser granular deposits, vesicles or curveted lamellae.

The biochemical composition of gangliosides of the central nervous system of mammals is well known and characterized by GM1, GD1a, GD1b, GT1b, GQ1b and small amount of GM3 and GD3; these are present in proportions approximately preserved in different species and correspond to different sialylation stages of the neutral chain Gal-GalNAc-Gal-Glc-Ceramide[48]. Gangliosides are catabolized in the lysosomes by glycohydrolases that are exclusively exoglycosidases, the sequence of hydrolysis is: GQ1b> GT1b> GD1a> GM1> GM2> GM3> LacCer> GlcCer> Cer>Sph and fatty acids[49]. Lysosomal diseases are most frequently classified according to the major storage compound[50]. For differentiation of gangliosidosis, biochemical analysis of the storage material with quantification of the different compounds can be a useful diagnostic and research tool[51]. GM1 gangliosidosis is characterized by the accumulation of GM1, GA1, GM2, GM3, GD1A, lyso-GM1, glucosylceramide, lactosylceramide, oligosaccharides and keratan sulphate[52].GM2 gangliosidosis, characterized by lack of hexosaminidase activity (necessary to pass from GM2 to GM3), is characterized by storage of GM2 ganglioside[52] and GalNAc-GD1a[53]. However, there are differences between Tay-Sachs and Sandhoff diseases in the storage gangliosides: the first has an increase in the content of GA2 and lyso-GM2, while the second has

increased globoside, oligosaccharides and lyso-GM2 portions[50]. Biochemical analysis, showed a striking increase of GM2 ganglioside in the brain of the affected wild boars, compared to age- and sex-matched normal animals; this result allows to confirm the diagnosis of GM2 gangliosidosis. Furthermore, ganglioside GalNAc-GD1a was also increased; this could be determined by its GalNAc-(Neu5Ac-)Gal terminal sequence, which is similar to GM2 ganglioside. HPTLC highlighted also an increase of trihexosylceramide; this can happen when GM2 accumulates, because sialidase finds a high concentration of substrate and is partially able to work by detaching the sialic acid, leaving the neutral trihexosylceramide. Drastic reduction of principal components of myelin (sphingomyelin, sulphatide and cerebrosides) was evident in the Or.Ph. analysis, as seen in the histological analysis and confirmed this disease as a possible model of dysmyelinogenesis[4].

Affected animals carried a variant in *HEXA* characteristic of Tay-Sachs disease. The missense variant altered the sequence of codon 499 and results in the replacement of arginine by cysteine (p.Arg499Cys). Multiple species amino acid sequence alignment showed that the wild type residue at the affected position is highly conserved across *HEXA* orthologues in vertebrates. This is probably due to important role of αArg499 which participates in hydrogen bonding with αGlu482 that furthermore bonds with αTrp26 of domain I; this salt-bridge is surrounded by hydrophobic residues, that comprise the interface between domain I and domain II of Hex A. Interaction between these domains plays a role in protein folding and/or facilitates dimer formation; thus, modification in αArg499 can lead to deleterious alteration of interaction between domain I and domain II of Hex A[54]. Furthermore, this is a CpG site, known to be “mutagenic hot spots”[55].

In human and other species, pathogenic *HEXA* variants are known to be associated with the disease. In human the p.Arg499Cys substitution resulting

from a C-to-T transition at nucleotide 1495 in exon 13 (rs121907966), is present in only 1 out of 251462 (GnomAD_exome) and 1 out of 125568 (TOPMED) patients. This missense variant has been found in different Tay-Sachs patients: in a homozygous state in one infantile case and in a compound heterozygous state in three infantile/late infantile cases and one adult-onset case[56–60].

A missense variant with substitution of histidine for arginine (p.Arg499His, rs121907956) in the same aminoacidic residue has been reported mainly in juvenile onset patients [55,58,61–63]. Human patients affected by both these variants have attenuated phenotypes[58]. The cysteine residue at position 499 (p.Arg499Cys) might create an illegitimate disulfide bridge in the protein with a resultant disruption of the normal three-dimensional structure, causing a more severe clinical phenotype than in histidine substitution (p.Arg499His)[57], where the α-chain generated is unstable but a small amount of mature polypeptide is produced[58].

Therefore, in the light of pathological and biochemical findings detected in the affected wild boars, the identified amino acid exchange represents the most likely pathogenic variant. Furthermore, this variant has been described in several affected human patients, highlighting that these animals might represent possible models for human Tay-Sachs disease.

The detection of an absent or reduced Hex A enzyme activity confirms the diagnosis of Tay–Sachs disease at a biochemical enzymatic level[75]. The use of artificial fluorescent substrates allows the assessment of the functionality of both Hex A and Hex B[18]. Furthermore, it has been demonstrated that the heterogeneity of onset correlates inversely with the residual catabolic activity of Hex A[75,76]. Human patients with an acute presentation have absent or very low (<5%) enzyme activity, while patients with subacute or chronic onset may have enzyme activities between 5% and 10%[18,75]. In patients with p.Arg499Cys aminoacidic substitution, the Hex A activity is reduced to less than

5% of the normal reference range[59]. In affected wild boars, carrying the same p.Arg499Cys mutation as human patients, Hex A enzyme activity was less than 1% of the tested healthy control animals, in line with data for humans patients. The mainstay of diagnosis for human patients, relies on enzymatic assay of β-hexosaminidase activities; these methods provided comparable results between affected wild boars and humans patients, with same aminoacidic substitution. Furthermore, biochemical enzymatic assays could be used to track the progress of the disease in wild boar models subjected to experimental treatments.

Though GM2 gangliosidosis has been reported in numerous species, only mice, cats, and sheep are established and maintained as research models[6,64]. The ovine model is currently the only available large animal model of Tay–Sachs disease; animals are characterized by a homozygous recessive missense (G to C transition) mutation, at nucleotide position 1330, which result in an amino acid change from Gly444 to Arg[10], associated with reduced enzyme activity (29% compared to controls) and juvenile onset of neurological disease. Clinical manifestations, like ataxia, proprioceptive defects and cortical blindness, are similar to the pathological features in humans[34]. This animal model has measurable clinical symptoms, is suited for surgical interventions and, as long-lived animals, for clinical evaluation over many years[65].

However, sheep have disproportionately larger body versus brain sizes, compared with humans, meaning that systemic therapies may not be effectively modeled in sheep. Additional disadvantages include the possession of horns (up to six in Jacob sheep), which creates challenges with imaging modalities, such as MRI and computed tomography [6].

Wild boars have several advantages some of which are similar to other large animal models, such as the possibility of breeding groups of animals with identical disease-causing mutations with a varied genetic background and the availability of fluids and tissue samples taken over long periods. This can lead to

a better understanding of the disease pathogenesis and the development of markers to track disease severity. Large long-lived animals are also suitable for biodistribution studies and studies on experimental therapy delivery as well as long-term safety and efficacy studies [64].

Wild boars also have peculiar characteristics, which can delineate a better large animal model for Tay–Sachs disease. Brain growth, composition, and myelination during its development around birth, in pigs, is similar to human[66] and sex-specific development [67]. These features allow to better understand pathogenesis and progression of the disease, which can be evaluated using non-invasive imaging methods, identical to those used in human diagnostics[67]. Several therapeutic approaches lack large animal model evaluation, which is fundamental to confirm efficacy and define dosing, in prospective human clinical trials[68]. Swine have been widely used in preclinical safety studies[69] and this spontaneous model of Tay–Sachs disease could be suitable for evaluation of the latest treatment proposals, defining evidences for translation to human patients. Gene therapy approaches, where distribution achieved upon local administration is likely dependent on brain size and structure, can be greatly improved by the use of this model, with better prediction of intrathecal and thalamic gene delivery[70]. Therapies based on CRISPR/Cas9 are still on initial stages; however, this genome editing tool is already an established method to manipulate the porcine genome, in order to create appropriate transgenic disease models[71]. Epigenetic editing, which combines epigenetic enzymes with the advantages of DNA-targeting techniques [72], represents a novel treatment alternative[73]. Established porcine methylation profiles, which are similar to those observed in humans[74], associated with the causative point mutation of the wild boars, affecting a CpG site, could give more insight on this innovative gene-based therapy.

Based on the presented results, these wild boars could be suitable to generate a research model colony. This is based on the confirmed possibility of screening carrier animals, with molecular identification of the missense variant, and quantification of enzyme activity in all animals, with biochemical tracking of the enzyme functionality during therapeutic approaches.

However, further studies are needed to better characterize pathological findings, such as inflammation and Blood-Brain Barrier (BBB) integrity, in order to clarify human relevance of the features identified in this spontaneous Tay-Sachs disease model.

5. Conclusion

Morphological, ultrastructural, biochemical and genetic features of GM2 gangliosidosis in three wild boars of the same litter were evaluated. These animals presented with neurological signs at 6 months of age; gross examination of brains showed reduction in parenchyma consistency. Severely enlarged neurons, characterized by foamy vacuolated cytoplasm, spheroids, meganeurite, astrogliosis, microgliosis and demyelination were morphological hallmarks of the pathology. TEM revealed the presence of elevated amount of cytoplasmic membranous bodies, characteristic of gangliosides storage. In affected animals, analyses of the lipid content of CNS detected the presence of an elevated amount of GM2 ganglioside and their Hex A enzyme activity in lymphocytes was less than 1%, compared to control animals. These results lead to the diagnosis of GM2 gangliosidosis. Genetical analysis demonstrated a missense variant resulting in the replacement of arginine by cysteine (p.Arg499Cys) in the hexosaminidase subunit alpha gene (*HEXA*), allowing the subclassification of Tay-Sachs disease. This variant has been described in different human patients that were affected by the aforementioned disease, suggesting that wild boars may be a suitable model to study the disease. Lysosomal storage diseases, such as Tay-Sachs, are relatively rare and

induced animal models have several limitations, due to possible differences with human pathologies; thus, spontaneous animal models, strictly similar to human disease, are indispensable tools. Presented results highlight that affected wild boars could be suitable for the development of a research model colony, for the study of the pathogenesis of Tay-Sachs and the development of potential treatments, in a tight interdisciplinary cooperation between the fields of human and veterinary medicine.

Acknowledgements

We acknowledge:

The laboratories of Pathology, Anatomy and Biochemistry of the Veterinary Medicine department, University of Parma, for their technical support.

The Next Generation Sequencing Platform of the University of Bern for performing the sequencing experiments and the Interfaculty Bioinformatics Unit of the University of Bern for providing computational infrastructure.

The AMMeC (Associazione Malattie Metaboliche Congenite, Italy) for their kind support.

Funding

This research did not receive any specific grant from funding agencies in the public, commercial, or not-for-profit sectors.

References

[1] L. Svennerholm, J.E. Månsson, Y.T. Li, Isolation and structural determination of a novel ganglioside, a disialosylpentahexosylceramide from human brain., J. Biol. Chem. (1973).
[2] T. Kolter, K. Sandhoff, Sphingolipid metabolism diseases, Biochim. Biophys. Acta - Biomembr. 1758 (2006) 2057–2079. doi:10.1016/j.bbamem.2006.05.027.
[3] T. Kolter, K. Sandhoff, Sphingolipid metabolism diseases, Biochim. Biophys. Acta - Biomembr. 1758 (2006) 2057–2079. doi:10.1016/j.bbamem.2006.05.027.
[4] D. Valle, A.L. Beaudet, B. Vogelstein, K.W. Kinzler, S.E. Antonarakis, A. Ballabio, K.M. Gibson, G. Mitchell, The online metabolic and molecular bases of inherited disease, (2016).
[5] NCBI, NCBI ClinVar, (2018). https://www.ncbi.nlm.nih.gov/clinvar.
[6] C.A. Lawson, D.R. Martin, Animal models of GM2 gangliosidosis: Utility and limitations, Appl. Clin. Genet. 9 (2016) 111–120.

doi:10.2147/TACG.S85354.

[7] C. Bertoni, Y.T. Li, S.C. Li, Catabolism of asialo-GM2 in man and mouse. Specificity of human/mouse chimeric GM2 activator proteins, J. Biol. Chem. 274 (1999) 28612–28618. doi:10.1074/jbc.274.40.28612.

[8] J.A. Yuziuk, C. Bertoni, T. Beccari, A. Orlacchio, Y.Y. Wu, S.C. Li, Y.T. Li, Specificity of mouse G(M2) activator protein and β-N-acetylhexosaminidases A and B. Similarities and differences with their human counterparts in the catabolism of G(M2), J. Biol. Chem. 273 (1998) 66–72. doi:10.1074/jbc.273.1.66.

[9] A.C. Freeman, S.R. Platt, M. Vandenberg, S. Holmes, M. Kent, R. Rech, E. Howerth, S. Mishra, D.P. O'Brien, D. Wenger, GM2 Gangliosidosis (B Variant) in Two Japanese Chins: Clinical, Magnetic Resonance Imaging and Pathological Characteristics, J. Vet. Intern. Med. 27 (2013) 771–776. doi:10.1111/jvim.12118.

[10] P.A. Torres, B.J. Zeng, B.F. Porter, J. Alroy, F. Horak, J. Horak, E.H. Kolodny, Tay-Sachs disease in Jacob sheep, Mol. Genet. Metab. 101 (2010) 357–363. doi:10.1016/j.ymgme.2010.08.006.

[11] M.E. Wessels, J.P. Holmes, M. Jeffrey, M. Jackson, A. Mackintosh, E.H. Kolodny, B.J. Zeng, C.B. Wang, S.F.E. Scholes, GM2ganglioside in British Jacob sheep, J. Comp. Pathol. 150 (2014) 253–257. doi:10.1016/j.jcpa.2013.10.003.

[12] T. Rickmeyer, S. Schöniger, A. Petermann, K. Harzer, B. Kustermann-Kuhn, H. Fuhrmann, H.A. Schoon, GM2 Gangliosidosis in an Adult Pet Rabbit, J. Comp. Pathol. 148 (2013) 243–247. doi:10.1016/j.jcpa.2012.06.008.

[13] S.D. Kosanke, K.R. Pierce, W.W. Bay, Clinical and Biochemical Abnormalities in Porcine GM2 Gangliosidosis, Vet. Pathol. 15 (1978) 685–699. doi:10.1177/030098587801500601.

[14] B.J. Zeng, P.A. Torres, T.C. Viner, Z.H. Wang, S.S. Raghavan, J. Alroy, G.M. Pastores, E.H. Kolodny, Spontaneous appearance of Tay-Sachs disease in an animal model, Mol. Genet. Metab. 95 (2008) 59–65. doi:10.1016/j.ymgme.2008.06.010.

[15] J. Fox, Y.-T. Li, G. Dawson, A. Alleman, J. Johnsrude, J. Schumacher, B. Homer, Naturally occurring G M2 gangliosidosis in two Muntjak deer with pathological and biochemical features of human classical Tay-Sachs disease (type B G M2 gangliosidosis), Acta Neuropathol. 97 (1999) 57–62. doi:10.1007/s004010050955.

[16] D.N. Sanders, R. Zeng, D.A. Wenger, G.S. Johnson, G.C. Johnson, J.E. Decker, M.L. Katz, S.R. Platt, D.P. O'Brien, GM2 gangliosidosis associated with a HEXA missense mutation in Japanese Chin dogs: A potential model for Tay Sachs disease, Mol. Genet. Metab. 108 (2013) 70–75. doi:10.1016/j.ymgme.2012.11.008.

[17] A.R. Pinnapureddy, C. Stayner, J. McEwan, O. Baddeley, J. Forman, M.R. Eccles, Large animal models of rare genetic disorders: Sheep as phenotypically relevant models of human genetic disease, Orphanet J. Rare Dis. 10 (2015). doi:10.1186/s13023-015-0327-5.

[18] M.B. Cachon-Gonzalez, E. Zaccariotto, T.M. Cox, Genetics and Therapies for GM2 Gangliosidosis., Curr. Gene Ther. (2018). doi:10.2174/1566523218666180404162622.

[19] H.L. Gray-Edwards, A.N. Randle, S.A. Maitland, H.R. Benatti, S.M. Hubbard, P.F. Canning, M.B. Vogel, B.L. Brunson, M. Hwang, L.E. Ellis, A.M. Bradbury, A.S. Gentry, A.R. Taylor, A.A. Wooldridge, D.R. Wilhite, R.L. Winter, B.K. Whitlock, J.A. Johnson, M. Holland, N. Salibi, R.J. Beyers, J.L. Sartin, T.S. Denney, N.R. Cox, M. Sena-Esteves, D.R. Martin, Adeno-Associated Virus Gene Therapy in a Sheep Model of Tay–Sachs Disease, Hum. Gene Ther. (2017) hum.2017.163.

doi:10.1089/hum.2017.163.
[20] S. Leary, W. Underwood, R. Anthony, S. Cartner, AVMA Guidelines for the Euthanasia of Animals: 2013 Edition, 2013. doi:10.1016/B978-012088449-0.50009-1.
[21] H.A. Yoon, K.E. Seong, A.G. Aleyas, O.P. Seong, J.H. Lee, S.C. Joon, G.C. Jeong, H.J. Song, Molecular survey of latent pseudorabies virus infection in nervous tissues of slaughtered pigs by nested and real-time PCR, J. Microbiol. (2005).
[22] B. Hoffmann, M. Beer, C. Schelp, H. Schirrmeier, K. Depner, Validation of a real-time RT-PCR assay for sensitive and specific detection of classical swine fever, J. Virol. Methods. (2005). doi:10.1016/j.jviromet.2005.05.030.
[23] J.A. Ramos-Vara, M. Kiupel, T. Baszier, L. Bliven, B. Brodersen, B. Chelack, S. Czub, F. Del Piero, S. Dial, E.J. Ehrhart, T. Graham, L. Manning, D. Paulsen, V.E. Valli, K. West, Suggested guidelines for immunohistochemical techniques in veterinary diagnostic laboratories, J. Vet. Diagnostic Investig. 20 (2008) 393–413. doi:10.1177/104063870802000401.
[24] N.F. Cheville, J. Stasko, Techniques in Electron Microscopy of Animal Tissue, Vet. Pathol. 51 (2014) 28–41. doi:10.1177/0300985813505114.
[25] C.T. Rueden, J. Schindelin, M.C. Hiner, B.E. DeZonia, A.E. Walter, E.T. Arena, K.W. Eliceiri, ImageJ2: ImageJ for the next generation of scientific image data, BMC Bioinformatics. 18 (2017). doi:10.1186/s12859-017-1934-z.
[26] C.A. Schneider, W.S. Rasband, K.W. Eliceiri, NIH Image to ImageJ: 25 years of image analysis, Nat. Methods. (2012). doi:10.1038/nmeth.2089.
[27] J. Schindelin, C.T. Rueden, M.C. Hiner, K.W. Eliceiri, The ImageJ ecosystem: An open platform for biomedical image analysis, Mol. Reprod. Dev. (2015). doi:10.1002/mrd.22489.
[28] F. Scandroglio, N. Loberto, M. Valsecchi, V. Chigorno, A. Prinetti, S. Sonnino, Thin layer chromatography of gangliosides, Glycoconj. J. 26 (2009) 961–973. doi:10.1007/s10719-008-9145-5.
[29] H. Kresse, W. Fuchs, J. Glössl, D. Holtfrerich, W. Gilberg, Liberation of N-acetylglucosamine-6-sulfate by human beta-N-acetylhexosaminidase A., J. Biol. Chem. 256 (1981) 12926–12932.
[30] H. Galjaard, Genetic metabolic diseases : early diagnosis and prenatal analysis, Amsterdam ; New York : Elsevier/North-Holland Biomedical Press ; New York : sole distributors for the U.S.A. and Canada, 1980. http://lib.ugent.be/catalog/rug01:000040794.
[31] A. Caciotti, S.C. Garman, Y. Rivera-Colón, E. Procopio, S. Catarzi, L. Ferri, C. Guido, P. Martelli, R. Parini, D. Antuzzi, R. Battini, M. Sibilio, A. Simonati, E. Fontana, A. Salviati, G. Akinci, C. Cereda, C. Dionisi-Vici, F. Deodato, A. d'Amico, A. d'Azzo, E. Bertini, M. Filocamo, M. Scarpa, M. di Rocco, C.J. Tifft, F. Ciani, S. Gasperini, E. Pasquini, R. Guerrini, M.A. Donati, A. Morrone, GM1 gangliosidosis and Morquio B disease: An update on genetic alterations and clinical findings, Biochim. Biophys. Acta - Mol. Basis Dis. (2011). doi:10.1016/j.bbadis.2011.03.018.
[32] A. Grahofer, A. Letko, I.M. Häfliger, V. Jagannathan, A. Ducos, O. Richard, V. Peter, H. Nathues, C. Drögemüller, Chromosomal imbalance in pigs showing a syndromic form of cleft palate, BMC Genomics. (2019). doi:10.1186/s12864-019-5711-4.
[33] S. Richards, N. Aziz, S. Bale, D. Bick, S. Das, J. Gastier-Foster, W.W. Grody, M. Hegde, E. Lyon, E. Spector, K. Voelkerding, H.L. Rehm, Standards and guidelines for the interpretation of sequence variants: A joint consensus recommendation of the American College of Medical Genetics and Genomics and the Association for Molecular Pathology, Genet. Med. (2015). doi:10.1038/gim.2015.30.

[34] B.F. Porter, B.C. Lewis, J.F. Edwards, J. Alroy, B.J. Zeng, P.A. Torres, K.N. Bretzlaff, E.H. Kolodny, Pathology of GM2 gangliosidosis in Jacob sheep, Vet. Pathol. (2011). doi:10.1177/0300985810388522.
[35] A.E. Bley, O.A. Giannikopoulos, D. Hayden, K. Kubilus, C.J. Tifft, F.S. Eichler, Natural history of infantile G M2 gangliosidosis, Pediatrics. (2011). doi:10.1542/peds.2011-0078.
[36] R.A. Sobel, Greenfield's Neuropathology, Ninth Edition, J. Neuropathol. Exp. Neurol. (2015). doi:10.1097/nen.0000000000000267.
[37] S.U. Walkley, Cellular pathology of lysosomal storage disorders., Brain Pathol. 8 (1998) 175–193. doi:10.1111/j.1750-3639.1998.tb00144.x.
[38] S.U. Walkley, H.J. Baker, M.C. Rattazzi, M.E. Haskins, J.Y. Wu, Neuroaxonal dystrophy in neuronal storage disorders: Evidence for major GABAergic neuron involvement, J. Neurol. Sci. (1991). doi:10.1016/0022-510X(91)90208-O.
[39] R. Myerowitz, Molecular pathophysiology in Tay-Sachs and Sandhoff diseases as revealed by gene expression profiling, Hum. Mol. Genet. (2002). doi:10.1093/hmg/11.11.1343.
[40] M. Jeyakumar, R. Thomas, E. Elliot-Smith, D.A. Smith, A.C. Van der Spoel, A. D'Azzo, V.H. Perry, T.D. Butters, R.A. Dwek, F.M. Platt, Central nervous system inflammation is a hallmark of pathogenesis in mouse models of GM1 and GM2 gangliosidosis, Brain. (2003). doi:10.1093/brain/awg089.
[41] R.D. Folkerth, Abnormalities of developing white matter in lysosomal storage diseases, J. Neuropathol. Exp. Neurol. (1999). doi:10.1097/00005072-199909000-00001.
[42] F. -C Chiu, W.T. Norton, K.L. Fields, The Cytoskeleton of Primary Astrocytes in Culture Contains Actin, Glial Fibrillary Acidic Protein, and the Fibroblast-Type Filament Protein, Vimentin, J. Neurochem. (1981). doi:10.1111/j.1471-4159.1981.tb05302.x.
[43] F. Seehusen, E.A. Orlando, K. Wewetzer, W. Baumgärtner, Vimentin-positive astrocytes in canine distemper: A target for canine distemper virus especially in chronic demyelinating lesions?, Acta Neuropathol. (2007). doi:10.1007/s00401-007-0307-5.
[44] M. V. Sofroniew, H. V. Vinters, Astrocytes: Biology and pathology, Acta Neuropathol. (2010). doi:10.1007/s00401-009-0619-8.
[45] E.M. Hol, M. Pekny, Glial fibrillary acidic protein (GFAP) and the astrocyte intermediate filament system in diseases of the central nervous system, Curr. Opin. Cell Biol. (2015). doi:10.1016/j.ceb.2015.02.004.
[46] K. V. Rama Rao, T. Kielian, Astrocytes and lysosomal storage diseases, Neuroscience. (2016). doi:10.1016/j.neuroscience.2015.05.061.
[47] E.J. Parkinson-Lawrence, T. Shandala, M. Prodoehl, R. Plew, G.N. Borlace, D.A. Brooks, Lysosomal Storage Disease: Revealing Lysosomal Function and Physiology, Physiology. (2010). doi:10.1152/physiol.00041.2009.
[48] T. Kolter, Ganglioside Biochemistry, ISRN Biochem. 2012 (2012) 1–36. doi:10.5402/2012/506160.
[49] T. Kolter, K. Sandhoff, Lysosomal degradation of membrane lipids, FEBS Lett. 584 (2010) 1700–1712. doi:10.1016/j.febslet.2009.10.021.
[50] A. Ballabio, V. Gieselmann, Lysosomal disorders: From storage to cellular damage, Biochim. Biophys. Acta - Mol. Cell Res. (2009). doi:10.1016/j.bbamcr.2008.12.001.
[51] T. Kobayashi, I. Goto, S. Okada, T. Orii, K. Ohno, T. Nakano, Accumulation of Lysosphingolipids in Tissues from Patients with GM1 and GM2 Gangliosidoses, J. Neurochem. (1992). doi:10.1111/j.1471-4159.1992.tb08460.x.
[52] B. Breiden, K. Sandhoff, Mechanism of secondary ganglioside and lipid

accumulation in lysosomal disease, Int. J. Mol. Sci. (2020). doi:10.3390/ijms21072566.
[53] B. Breiden, K. Sandhoff, Lysosomal glycosphingolipid storage diseases, Annu. Rev. Biochem. (2019). doi:10.1146/annurev-biochem-013118-111518.
[54] M.J. Lemieux, B.L. Mark, M.M. Cherney, S.G. Withers, D.J. Mahuran, M.N.G. James, Crystallographic Structure of Human β-Hexosaminidase A: Interpretation of Tay-Sachs Mutations and Loss of GM2 Ganglioside Hydrolysis, J. Mol. Biol. (2006). doi:10.1016/j.jmb.2006.04.004.
[55] B.H. Paw, S.M. Moskowitz, N. Uhrhammer, N. Wright, M.M. Kaback, E.F. Neufeld, Juvenile G(M2) gangliosidosis caused by substitution of histidine for arginine at position 499 or 504 of the α-subunit of β-hexosaminidase, J. Biol. Chem. (1990).
[56] E.H. Mules, S. Hayflick, C.S. Miller, L.W. Reynolds, G.H. Thomas, Six novel deleterious and three neutral mutations in the gene encoding the alpha-subunit of hexosaminidase A in non-Jewish individuals., Am. J. Hum. Genet. (1992).
[57] S. Akli, J.C. Chomel, J.M. Lacorte, L. Bachner, J. Kahn, L. Poenaru, Ten novel mutations in the HEXA gene in non-jewish tay-sachs patients, Hum. Mol. Genet. (1993). doi:10.1093/hmg/2.4.496.
[58] A. Tanaka, L.T.N. Hoang, Y. Nishi, S. Maniwa, M. Oka, T. Yamano, Different attenuated phenotypes of GM2 gangliosidosis variant B in Japanese patients with HEXA mutations at codon 499, and five novel mutations responsible for infantile acute form, J. Hum. Genet. 48 (2003) 571–574. doi:10.1007/s10038-003-0080-9.
[59] G.H.B. Maegawa, T. Stockley, M. Tropak, B. Banwell, S. Blaser, F. Kok, R. Giugliani, D. Mahuran, J.T.R. Clarke, The natural history of juvenile or subacute GM2 gangliosidosis: 21 New cases and literature review of 134 previously reported, Pediatrics. (2006). doi:10.1542/peds.2006-0588.
[60] L. Gort, N. De Olano, J. Macías-Vidal, M.J. Coll, GM2 gangliosidoses in Spain: Analysis of the HEXA and HEXB genes in 34 Tay-Sachs and 14 Sandhoff patients, Gene. (2012). doi:10.1016/j.gene.2012.06.080.
[61] S. Zampieri, A. Montalvo, M. Blanco, I. Zanin, H. Amartino, K. Vlahovicek, M. Szlago, A. Schenone, G. Pittis, B. Bembi, A. Dardis, Molecular analysis of HEXA gene in Argentinean patients affected with Tay-Sachs disease: Possible common origin of the prevalent c.459+5A>G mutation, Gene. (2012). doi:10.1016/j.gene.2012.03.022.
[62] B.H. Paw, L.C. Wood, E.F. Neufeld, A third mutation at the CpG dinucleotide of codon 504 and a silent mutation at codon 506 of the HEX A gene., Am. J. Hum. Genet. 48 (1991) 1139–46. http://www.pubmedcentral.nih.gov/articlerender.fcgi?artid=1683090&tool=pmcentrez&rendertype=abstract.
[63] J.D. Hoffman, V. Greger, E.T. Strovel, M.G. Blitzer, M.A. Umbarger, C. Kennedy, B. Bishop, P. Saunders, G.J. Porreca, J. Schienda, J. Davie, S. Hallam, C. Towne, Next-generation DNA sequencing of HEXA: A step in the right direction for carrier screening, Mol. Genet. Genomic Med. (2013). doi:10.1002/mgg3.37.
[64] B.L. Gurda, C.H. Vite, Large animal models contribute to the development of therapies for central and peripheral nervous system dysfunction in patients with lysosomal storage diseases, Hum. Mol. Genet. (2019). doi:10.1093/hmg/ddz127.
[65] M.B. Cachon-Gonzalez, E. Zaccariotto, T.M. Cox, Genetics and Therapies for GM2 Gangliosidosis., Curr. Gene Ther. (2018) 68–89. doi:10.2174/1566523218666180404162622.
[66] M.S. Conrad, R.N. Dilger, R.W. Johnson, Brain growth of the domestic pig (Sus scrofa) from 2 to 24 weeks of age: A longitudinal MRI study, Dev.

Neurosci. (2012). doi:10.1159/000339311.
[67] B. Hoffe, M.R. Holahan, The Use of Pigs as a Translational Model for Studying Neurodegenerative Diseases, Front. Physiol. (2019). doi:10.3389/fphys.2019.00838.
[68] V. V. Solovyeva, A.A. Shaimardanova, D.S. Chulpanova, K. V. Kitaeva, L. Chakrabarti, A.A. Rizvanov, New approaches to Tay-Sachs disease therapy, Front. Physiol. (2018). doi:10.3389/fphys.2018.01663.
[69] D. Dolezalova, M. Hruska-Plochan, C.R. Bjarkam, J.C.H. Sørensen, M. Cunningham, D. Weingarten, J.D. Ciacci, S. Juhas, J. Juhasova, J. Motlik, M.P. Hefferan, T. Hazel, K. Johe, C. Carromeu, A. Muotri, J. Bui, J. Strnadel, M. Marsala, Pig models of neurodegenerative disorders: Utilization in cell replacement-based preclinical safety and efficacy studies, J. Comp. Neurol. (2014). doi:10.1002/cne.23575.
[70] M.M. Evers, J. Miniarikova, S. Juhas, A. Vallès, B. Bohuslavova, J. Juhasova, H.K. Skalnikova, P. Vodicka, I. Valekova, C. Brouwers, B. Blits, J. Lubelski, H. Kovarova, Z. Ellederova, S.J. van Deventer, H. Petry, J. Motlik, P. Konstantinova, AAV5-miHTT Gene Therapy Demonstrates Broad Distribution and Strong Human Mutant Huntingtin Lowering in a Huntington's Disease Minipig Model, Mol. Ther. (2018). doi:10.1016/j.ymthe.2018.06.021.
[71] I.E. Holm, A.K.O. Alstrup, Y. Luo, Genetically modified pig models for neurodegenerative disorders, J. Pathol. (2016). doi:10.1002/path.4654.
[72] M.G.S. Rutten, M.G. Rots, M.H. Oosterveer, Exploiting epigenetics for the treatment of inborn errors of metabolism, J. Inherit. Metab. Dis. (2020). doi:10.1002/jimd.12093.
[73] S. Hassan, E. Sidransky, N. Tayebi, The role of epigenetics in lysosomal storage disorders: Uncharted territory, Mol. Genet. Metab. (2017). doi:10.1016/j.ymgme.2017.07.012.
[74] K.M. Schachtschneider, O. Madsen, C. Park, L.A. Rund, M.A.M. Groenen, L.B. Schook, Adult porcine genome-wide DNA methylation patterns support pigs as a biomedical model, BMC Genomics. (2015). doi:10.1186/s12864-015-1938-x.
[75] A.F. Leal, E. Benincore-Flórez, D. Solano-Galarza, R.G.G. Jaramillo, O.Y. Echeverri-Peña, D.A. Suarez, C.J. Alméciga-Díaz, A.J. Espejo-Mojica, Gm2 gangliosidoses: Clinical features, pathophysiological aspects, and current therapies, Int. J. Mol. Sci. (2020). doi:10.3390/ijms21176213.
[76] K. Sandhoff, K. Harzer, Gangliosides and gangliosidoses: Principles of molecular and metabolic pathogenesis, J. Neurosci. (2013). doi:10.1523/JNEUROSCI.0822-13.2013.